Synthesis and crystal structure determination of copper(II)-complex: In vitro DNA and HSA binding, pBR322 plasmid cleavage, cell imaging and cytotoxic studies

ARTICLE *in* EUROPEAN JOURNAL OF MEDICINAL CHEMISTRY · JUNE 2014

Impact Factor: 3.45 · DOI: 10.1016/j.ejmech.2014.06.018 · Source: PubMed

European Journal of Medicinal Chemistry 83 (2014) 141–154

Contents lists available at ScienceDirect

European Journal of Medicinal Chemistry

journal homepage: http://www.elsevier.com/locate/ejmech

Original article

Synthesis and crystal structure determination of copper(II)-complex: *In vitro* DNA and HSA binding, pBR322 plasmid cleavage, cell imaging and cytotoxic studies

Sartaj Tabassum [a, *], Mehvash Zaki [a], Musheer Ahmad [b], Mohd Afzal [a], Saurabh Srivastav [c], Saripella Srikrishna [c], Farukh Arjmand [a]

[a] Department of Chemistry, Aligarh Muslim University, Aligarh 202002, India
[b] Department of Chemistry, Indian Institute of Technology Kanpur, UP 208016, India
[c] Department of Biochemistry, Faculty of Science, Banaras Hindu University, Varanasi 221005, India

ARTICLE INFO

Article history:
Received 28 February 2014
Received in revised form
5 June 2014
Accepted 9 June 2014
Available online 10 June 2014

Keywords:
In vitro DNA binding
HSA binding
DNA cleavage
SDS-PAGE analysis
Topo-I inhibition
Anticancer activity

ABSTRACT

New Cu(II) complex **1** of indole-3-propionic acid and 1,10-phenanthroline was synthesized and characterized by analytical, spectroscopic and single crystal X-ray diffraction. *In vitro* DNA binding studies of **1** was performed by employing UV–vis and fluorescence spectroscopic techniques. The binding affinity towards human serum albumin (HSA) was also investigated to understand the carrier role in body system, as the time dependent HPLC experiment of **1** revealed that bonded drug with protein releases slowly in presence of DNA. Complex **1** exhibited good anti-tumor activity (GI_{50} values <10 μg/ml), and to elucidate the mechanism of tumor inhibition, topoisomerase I enzymatic activity was carried out and further validated by cell imaging studies which clearly showed its nuclear localization.

1. Introduction

Cancer is a class of multigenic disease characterized by a diversity of genetic and epigenetic alterations and become a leading cause of death worldwide which can be cured by preventing the rapid proliferation of cancer cells for which the replication of DNA is to be arrested [1]. The clinical success of cisplatin, *cis*-diamminedichloroplatinum(II), and other platinum-based drugs for treating solid malignant tumors has spurred research interest in medicinal inorganic chemistry. Inspite of the great success of cisplatin, nevertheless, the challenges for utility of cisplatin still remain due to severe systemic toxicity, intrinsic drug resistance (due to off-target binding of the drug) and high cost issues [2–4]. The molecular mechanism of action of such DNA-targeting drugs involves the formation of covalent binding to nucleobase moieties and a low degree of selectivity. Therefore, it was impertinent to understand the noncovalent interactions of transition metal complexes other than platinum with DNA that exhibit enhanced selectivity and to explore their structure–function relationship to cytotoxicity in tumor cells.

DNA has been identified as a primary intracellular target for anticancer drug design and remains one of the most promising biological receptors for the development of chemotherapeutic agents. The interaction between transition metal complexes and DNA could probably cause DNA damage in cancer cells, which in turn blocked cell division and finally results in cell death. Among them, copper complexes are a class of the most frequently studied metallonucleases due to their biologically accessible redox states [5]. Copper binds to DNA with high affinity than any other divalent cation, thus promoting DNA oxidation [6]. Since the discovery of the first chemical nuclease bis-phenanthroline copper complex $Cu(phen)_2^{2+}$, a number of artificial nucleases containing redox-active Cu(II) as their active sites have been synthesized which are essential for generating the reactive oxygen species (ROS) necessary for DNA cleavage [7]. Recently, Reedijk and co-workers have

Abbreviations: UV–vis, UV–visible; CT DNA, Calf thymus DNA; Tris, Tris(hydroxymethyl)aminomethane; EB, Ethidium bromide; Phen, 1,10-Phenanthroline; IPA, Indole-3-propionic acid.

* Corresponding author. Department of Chemistry, Aligarh Muslim University, Aligarh, UP 202002, India.
E-mail addresses: tsartaj62@yahoo.com, tsartaj62@gmail.com (S. Tabassum).

http://dx.doi.org/10.1016/j.ejmech.2014.06.018
0223-5234/

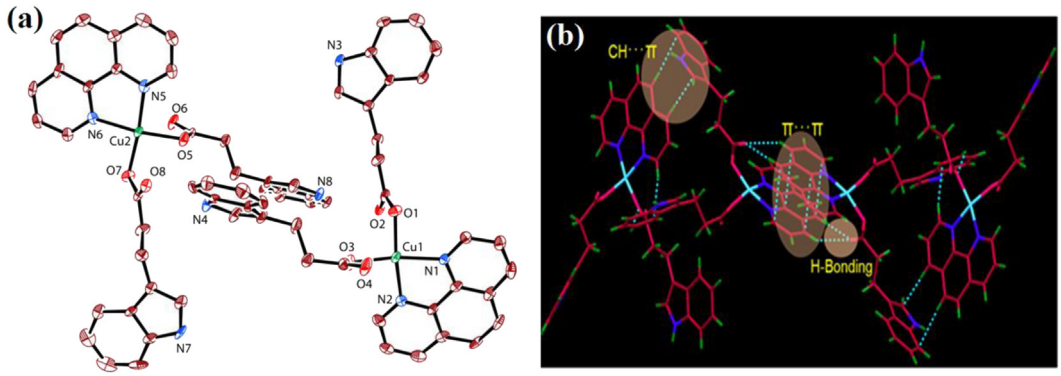

Fig. 1. Schematic representation of (a) asymmetric unit containing both molecules in ORTEP view and (b) non-covalent weak interactions in complex **1**.

reported that mononuclear copper complex shows efficient self-activated DNA cleavage activity and cytotoxic effects toward L1210 murine leukemia and A2780 human ovarian carcinoma cell lines [8]. On the other hand indole-3-propionic acid represents one of the most important heterocyclic compounds and many indole derivatives are found to exhibit diverse biological activities antibacterial, antifungal, antioxidant, analgesic, antiasthmatic, and antiviral and also found to be effective in treatment of cancer [9]. Due to its free radical scavenging and antioxidant properties, IPA acts as a potential therapeutic agent against carcinogenesis by protecting the cells against free-radical damage. However, the biological activity of indole derivatives has been considerably enhanced by binding with metal ions [10].

Topoisomerase are involved in many aspects of DNA metabolism and chromatin topology. Topoisomerase inhibitors are among the most active anticancer agents due to the critical role of these enzymes for the cell proliferative process. Literature reveals that minor groove analogs such as camptothecin, Hoechst 33258, bleomycin and netropsin (G–C recognition elements) were found to be potent anti-tumor drugs with a broad spectrum of antitumor activity due to their strong DNA Topo I inhibition [11]. Therefore, there is an overwhelming need to develop new topoisomerase inhibitors agents which exhibits different mode of action distinct from existing drugs.

Herein, we are reporting the synthesis, characterization and molecular docking of Cu(II)-based cancer chemotherapeutic drug entity (**1**). The complex (**1**) recognizes the DNA minor groove and inhibit the expression of Topo-I catalytic activity. To understand the drug–protein interaction, the affinity of **1** towards HSA was also investigated by the spectroscopic studies and also examined by HPLC experiment at different time interval. Furthermore, *in vitro* cytotoxicity of (**1**) was tested on a panel of human carcinoma cell lines (U373MG, A2780, K562, HCT15, MCF7, PC3, Hop62); additionally, intracellular localization was evidenced by cell imaging studies using HeLa cells.

2. Results and discussion

2.1. Spectroscopy

The IR spectrum of complex **1** exhibited strong bands at 1587 (ν_{asym} OCO) and 1337 cm^{-1} (ν_{sym} OCO) with $\Delta\nu$ values (250 cm^{-1}) indicating that carboxylate group was bonded to metal in a monodentate mode [12]. The bands at 849, 714 and 1492 cm^{-1} assigned to ν(C–H) (out-of-plane CH) and ν(C=N) of phenanthroline were shifted to lower frequencies compared to free phenanthroline revealing the coordination of phen N atoms with metal ion [13]. The medium intensity bands at 424 and 563 cm^{-1} were attributed to stretching vibration of ν(Cu–N) and ν(Cu–O), respectively.

The electronic spectra of complex exhibited high energy band at 270 nm and a shoulder band at 297 nm attributed to the intraligand π–π^* transitions of the aromatic chromophore of coordinated indole-3-propionic acid and 1,10-phenanthroline. In addition, a band at 367 nm was assigned to LMCT transition [14]. The low energy broad asymmetrical band in the visible region with a maximum appearing at 540 nm consistent with the square planar geometry around Cu(II) ion [15].

The liquid state X-band EPR spectrum of complex **1** was recorded in DMSO at liquid nitrogen temperature on X-band at frequency of 9.1 GHz under the magnetic field strength of 3000 ± 1000 Gauss using tetracyano ethylene (TCNE) as field marker as shown in Fig. 1. The EPR spectrum revealed an anisotropic signal with $g_{\|} = 2.26$, $g_{\perp} = 2.07$ and $g_{av} = 2.13$ computed from the expression $g_{av}^2 = (g_{\|}^2 + 2g_{\perp}^2)/3$, was observed. The trend $g_{\|} > g_{\perp} > 2.0023$ revealed that the unpaired electron most likely localized in $d_x^2 - {}^2_y$ orbital consistent with the square planar geometry [16].

2.2. Structure description

The complex **1** crystallizes in the monoclinic space group *P*21/*n* with two molecules in asymmetric unit. Each independent molecule in asymmetric unit of **1** consists of a Cu(II) metal ion, two IPA^{-1} ligands and one phen molecule (Fig. 1a). The metal shows slight distorted square planar geometry CuN_2O_2 coordination environment with ligation from two carboxylate oxygen (Cu–O = 1.920 (4)–1.925 (4) Å) from IPA^{-1} ligands and two nitrogen (Cu–N = 1.988 (5)–1.994 (5) Å) from phen ligand moiety.

The crystal structure shows a strong π–π aromatic stacking arrangement between two neighboring phen as well as between phen and indole moieties. The π–π aromatic stacking distances of the phen ligands are in range of 3.21–3.36 A°. These π–π aromatic interactions are further reinforced by both C–H···π and non-covalent H-bonding interactions to form an overall 3D supramolecular structure (Fig. 1b).

2.3. DNA binding studies

The interaction of transition metal complexes in a well-tailored ligand framework can complement the major/minor groove of the DNA double helix. Therefore, metal complex–DNA interactions are of considerable interest in the rational design and construction of new drugs targeted to DNA. The interaction of **1** with DNA was analyzed by a number of techniques, such as UV–Vis absorption fluorescence spectroscopic titration and viscosity measurements.

To determine the binding mode of complex **1** with calf thymus DNA (CT DNA), absorption titrations experiments were carried out. Upon addition of increasing concentration of DNA to the fixed concentration of **1**, a concomitant increase in the absorption intensity (hyperchromism) was observed (Fig. S1), implicating that **1** interact electrostatically with oxygen phosphate backbone of DNA duplex in addition to coordinate covalent binding *via* N7 atom of guanine nucleobases [17]. In general metal-complexes can bind to the DNA in different binding fashions on the basis of their, charge and type of ligands framework. DNA possesses several hydrogen bonding sites which are accessible both in major and minor grooves. So it is likely that –NH groups of indole ring form hydrogen bonding with the DNA base pairs. To quantify the extent of binding of complex **1** to CT DNA, the intrinsic binding constant, K_b was calculated by monitoring the changes in the absorbance at the corresponding λ_{max} with increasing concentrations of CT DNA and is given by the ratio of slope to the intercept in plots from the Wolfe–Shimer equation which was found to be 5.1×10^4 M^{-1}, indicating that **1** avidly binds to CT DNA due to presence of a large planar aromatic phenanthroline ligand which facilitates strong hydrophobic interactions with the DNA base pairs in addition to the hydrogen bonding interactions of the indole-3-propionic acid ligand. Moreover, the interaction of square planar Cu(II) complexes with DNA was stronger as compared to octahedral due to the fact that there is vacant coordination site available for the N7 position of guanine base pair to interact with metal ion [18].

The emission spectra of complex **1** displayed an intense luminescence at 336 nm in 0.01 Tris–HCl/50 mM NaCl buffer at room temperature in the absence of DNA when excited at 260 nm. On addition of increasing concentration of CT DNA (0.8×10^{-5} to 5.6×10^{-5} M) to fixed amount of complex **1**, emission intensity decreases remarkably by 94% with no apparent change in the shape and position of emission bands (Fig. S2). The quenching of the luminescence excited state of **1** was attributed to energy or electron transfer from the guanine base of DNA to the MLCT of complex [19]. This marked decrease in the emission intensity revealed either complete or partial intercalation into or electron/energy transfer with double-stranded DNA [20]. Moreover, quenching of fluorescence intensity was due to the enhanced shielding of complex **1** by binding with DNA from solvent water molecules thereby restricted the complex mobility at the binding site, leading to decrease in vibrational mode of relaxation.

The binding constant value K for complex **1** determined from Scatchard equation was calculated to be 5.7×10^4 M^{-1}, consistent with absorption titration studies.

In order to further examine the binding mode of complex **1** with DNA, competitive binding experiment using ethidium bromide (EB) as a probe was carried out. Ethidium bromide is a typical indicator of intercalation since it can form soluble complexes with nucleic acids emitting intense fluorescence in the presence of CT DNA due to the intercalation of the planar phenenthridinium ring between adjacent base pairs on the double helix. The enhanced fluorescence can be quenched upon the addition of the second molecule which could replace the bound EB or break the secondary structure of the DNA [21]. Upon addition of increasing concentration of **1** to CT DNA pretreated with EB ([DNA]/[EB] = 1) solution, the emission band at 591 nm exhibited quenching of the emission intensity up to 49% of the initial fluorescence intensity when the molar ratio of the complex to CT-DNA (r = [complex]/[CT-DNA]) range from 1.6 to 15.0 (Fig. S3). The observed decrease in the fluorescence intensity indicates that the EB molecule was displaced by the complex **1** from their DNA binding sites. Since EB was not completely displaced, partial intercalation in addition to the electrostatic mode of binding cannot be ruled out [22]. The extent of quenching of the emission intensity gives a measure of the binding propensity of the complex **1** to CT DNA. According to the classical Stern–Volmer equation:

$$\frac{I_o}{I} = 1 + K_{sv}r$$

where I_0 and I represent the fluorescence intensities in the absence and presence of the complex **1**, respectively; r is the concentration ratio of the complex to DNA and K_{SV} used to evaluate the quenching efficiency is obtained as the slope of I_0/I versus r and was found to be 5.88, indicating the interaction of complex **1** with CT DNA.

Viscosity titration measurements was carried out to examine the effect of complex **1** on the relative viscosity of DNA by keeping $[DNA] = 9.6 \times 10^{-6}$ constant and increasing [complex]/[DNA] ratios from 0.8 to 5. When the DNA helix was intercalated by planar molecules such as by classical intercalator EB, base pairs are separated to accommodate the binding molecule, resulting in the lengthening of the DNA helix and subsequently increased DNA viscosity. On contrary complexes bound to DNA through groove binding do not alter the relative viscosity of DNA whereas complexes that bound electrostatically will produce bend or kink the DNA helix, reducing its effective length and its viscosity, concomitantly [23]. On addition of increasing amount of complex **1,** the relative viscosity of CT DNA decreases which was comparable with the known intercalator ethidium bromide (EB) (which shows significant increase in relative viscosity) (Fig. S4). These results suggested that complex **1** was bound to CT DNA through electrostatic interaction leads to decreases in the relative viscosity.

2.4. DNA cleavage studies

Transition metal complexes are well suited for application as metallonucleases, because of their possibility to tune the redox potential through the choice of proper metal ion [24]. Therefore, in order to access the DNA cleavage ability of copper(II) complex **1**, supercoiled pBR322 DNA was incubated with increasing concentration of **1** in 5 mM Tris–HCl/40 mM NaCl buffer solution (pH 7.42) for 45 min in the absence of any external agents. The concentration dependent DNA cleavage activity of complex **1** was observed by gel electrophoresis as shown in Fig. S5. With increase in concentration of complex **1**, the amount of Form I of pBR322 DNA gradually diminishes whereas Form II increases, suggesting the single strand DNA cleavage [25]. At 25 μM concentration, complex **1** exhibited efficient nuclease activity and there was complete conversion of Form I into Form II. Quantification of the both the forms originating from SC and NC plasmids were visualized by using Vilber–INFINITY gel documentation system. It was remarkable to note that the amount of NC form in lane 6 was highest showing the maximum band area clearly indicting the concentration dependent cleavage of DNA by **1**.

The nuclease efficiency of metal complexes usually depends on the activators used for initiating the DNA cleavage process. Therefore, DNA cleavage activity of complex **1** was evaluated in the presence of H_2O_2, ascorbate (Asc), 3-mercaptopropionic acid (MPA) and glutathione (GSH) as shown in Fig. S6. Many copper (II) complexes can cleave DNA more efficiently in the presence of exogenous agents. The cleavage activity was significantly enhanced in the presence of these activators because of the reduction of Cu(II) complex to Cu(I) complex and the formation of Cu(I)-DNA adduct which further reacts with these reducing agents to generate reactive oxygen species responsible for the DNA cleavage and the cleavage activity follows the order $H_2O_2 \approx$ MPA > Asc > GSH. Thus complex **1** in presence of H_2O_2 and MPA exhibited significant DNA cleavage activity (Scheme 2), followed by complete degradation of DNA was observed, suggesting that these activators plays a role to

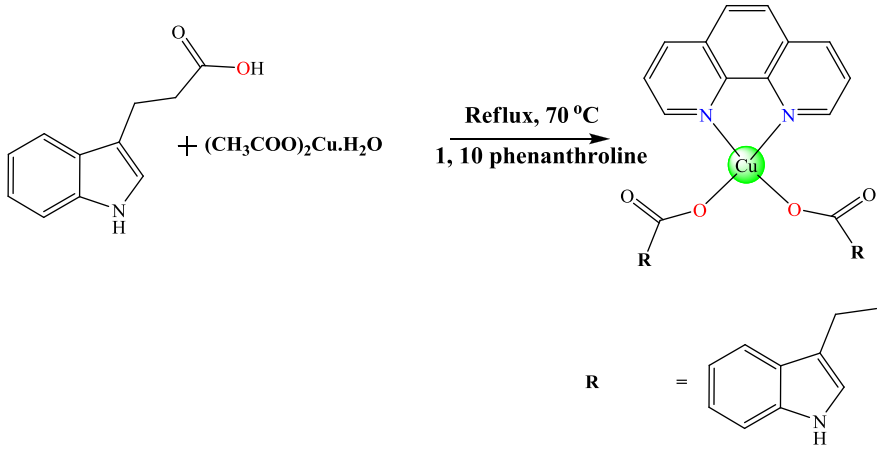

Scheme 1. Synthetic route to complex **1**.

aid the copper(II) complex in DNA degradation by oxidative cleavage.

In order to obtain information about the reactive oxygen species (ROS) which was responsible for the DNA cleavage catalyzed by complex **1**, reactions were investigated in the presence of standard radical scavengers such as hydroxyl radical scavengers (DMSO, EtOH), a singlet oxygen quencher (NaN_3) and a superoxide scavenger (SOD) under our experimental conditions (Fig. 2). On addition of DMSO and EtOH (lane 2 and 3), no obvious inhibition in the DNA cleavage activity was observed, suggesting that OH• radicals was not involved in the cleavage process. The SOD enzyme also has no effect on the cleavage reaction (lane 5), indicating the non-involvement of DNA cleavage by superoxide anion. However, in the presence of NaN_3, DNA cleavage was significantly diminished. These results suggested that Cu(I) species, singlet oxygen and hydroxyl radical OH• was the active species, responsible for DNA strand scission *via* oxidative pathway.

2.5. Topoisomerase I inhibition

A standard plasmid cleavage assay was used to investigate the effect of complex **1** on the activity of human Topo-I by agarose gel electrophoresis. This assay provides a direct means of determining whether the complex affects the unwinding of a supercoiled (SC) duplex DNA to nicked open circular (NOC) and relaxed (R) DNA. With increasing concentration of complex **1**, the levels of the relaxed form were diminished (Lanes 3–7, Fig. 3a). At 25 μM concentration of complex **1**, the DNA relaxation activity of Topo-I was significantly diminished (IC_{50} 20 μM) [26]. The results revealed that complex **1** may inhibited the Topo-I enzymatic activity either by (i) strong DNA binding and thereby preventing the binding of Topo-I to DNA and exercising its function, or (ii) binding to Topo-I and inactivating its proper functioning. Additionally, molecular technique docking was also employed to understand the binding mode of complex **1** with human–DNA–Topo-I complex (PDB ID: 1SC7). As depicted in Fig. 3b The docked model showed that complex **1** approaching towards the gap of DNA cleavage site in the Topo-I–DNA complex and forming a stable complex through π–π stacking interactions between the purine ring and pyrimidine ring in the minor groove on the scissile strand which may block the rewinding step of the phosphoester.

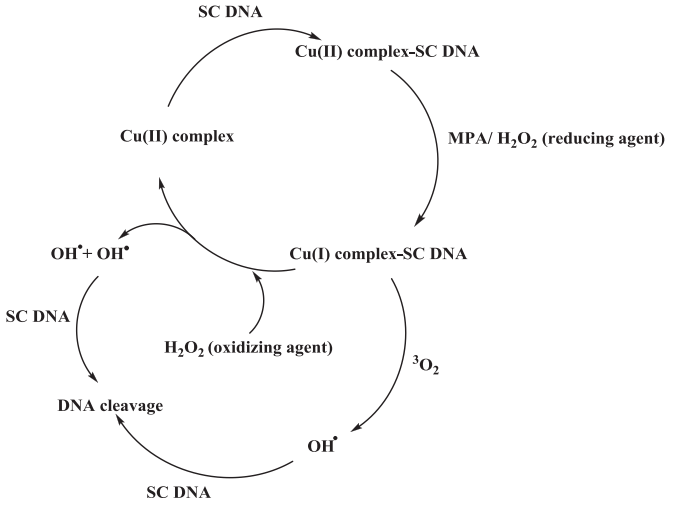

Scheme 2. Proposed mechanisms of DNA cleavage by complex $C_{34}H_{28}CuN_4O_4$ in the presence of activators.

2.6. HSA binding studies

The interaction of drug with blood plasma protein has attracted much interest in research, since serum albumin constitutes ~55% of the total blood plasma protein and plays a vital role in the drug transport (metal complexes) and drug metabolism. Therefore, it is interesting to explore the interaction studies of complex **1** with human serum albumin (HSA) by employing different spectral techniques.

Electronic absorption spectroscopy is a reliable tool to understand the structural changes in secondary structure of HSA and to establish complex formation between drug and HSA. Upon addition of complex **1** with an incremental increase in concentration ($0.67–4.0 \times 10^{-5}$ M) to HSA of constant concentration (0.67×10^{-6} M), a gradual increase in absorption intensity, hyperchromism of the intraligand band at 273 nm was observed (Fig. S7). The results implicates that the complex **1** interacted with HSA by non-covalent interaction most likely by electrostatic attraction and could be facilitated by hydrogen-bond formation, leads to the modulation in the absorption profile originating from the effect of the polar solvent (water) and perturbations in the micro-environment of the polypeptide backbone of the HSA. The intrinsic binding constant (K_b) of complex **1** with HSA was calculated using Eqs. (1)–(6)in supplementary material and was found to be 1.13×10^4 M^{-1}. The K_b value suggested that complex **1** has moderate binding propensity with HSA followed by conformational changes in its structure.

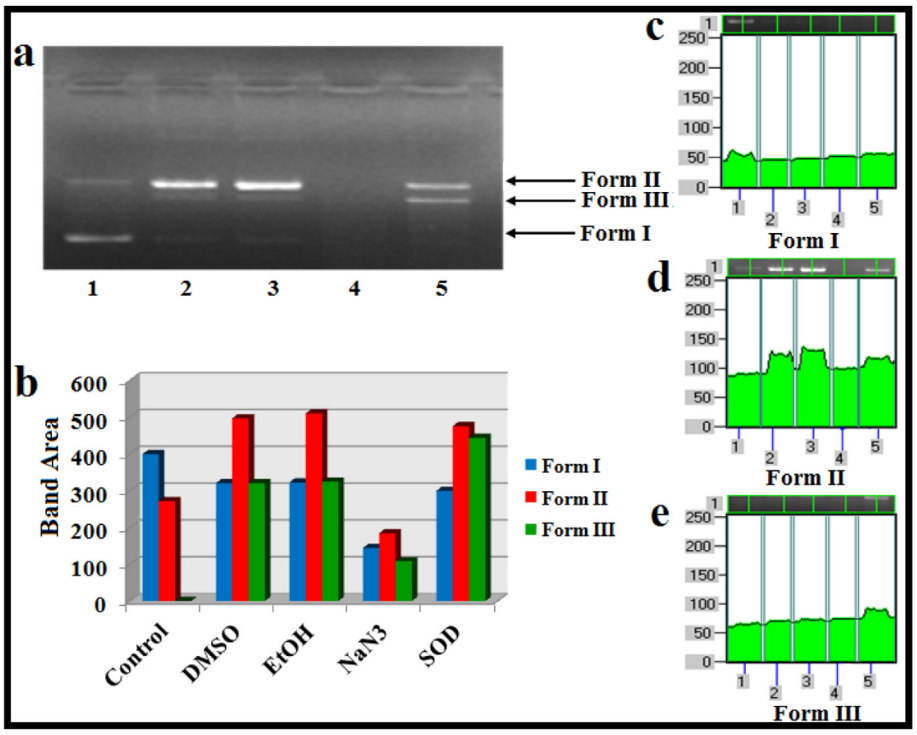

Fig. 2. Agarose gel electrophoresis pattern for the cleavage pattern of pBR322 DNA (300 ng) by complex **1** at 37 °C after incubation for 45 min in presence of (a) different radical scavengers; Lane 1, DNA control; Lane 2, DNA + complex **1** + DMSO (0.4 mM); Lane 3, DNA + complex **1** + EtOH (0.4 mM); Lane 4, DNA + complex **1** + NaN_3 (0.4 mM); Lane 5, DNA + complex **1** + SOD (0.25 mM); (b) Quantification of band area in gel electrophoresis originating from Form I and Form II pBR322 plasmid DNA by complex **1** in the presence of various radical scavengers. 2D projection of gel images for the cleavage of pBR322 plasmid DNA by complex **1** in presence of different radical scavengers (c) Form I, (d) Form II and (e) Form III bands.

The emission quenching experiment was carried out to study the interaction of Cu(II) complex with HSA as depicted in Fig. S8. The intrinsic fluorescence of HSA was dominated by mainly tryptophan residue at an emission wavelength of 362 nm; when small molecular substances bound to HSA, the changes of fluorescence intensity of HSA are induced by the microenvironment of Trp residue. The fluorescence spectra of HSA in the absence and presence of complex **1** as a quencher in Tris–HCl buffer (pH 7.4) was monitored with an excitation wavelength of 272 nm. On addition of increasing concentration of complex **1** (0.67×10^{-5} to 1.67×10^{-5} M) to fixed amount of HSA, intrinsic fluorescence intensity of HSA decreased gradually up to 67% accompanied by a

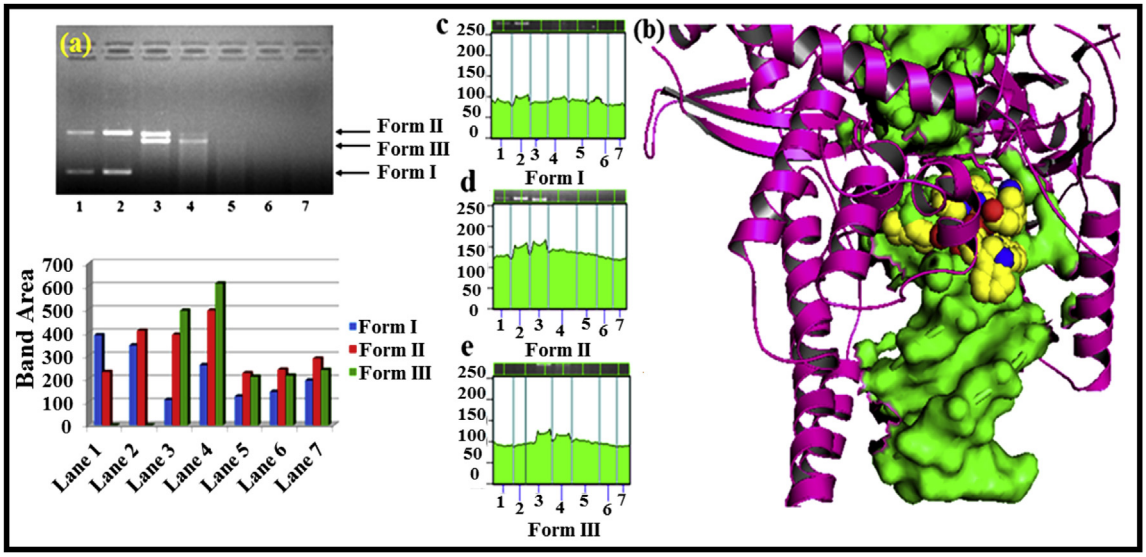

Fig. 3. Agarose gel electrophoresis with their quantification of band area originating from SC, NC and OC DNA in cleavage experiments showing the effect of different concentrations of complex **1** on the activity of (a) DNA topoisomerase I (Topo-I); Lane 1, DNA control; Lane 2, Topo-I + DNA; Lane 3, 5 μM **1** + DNA + Topo-I; Lane 4: 10 μM **1** + DNA + Topo-I; Lane 5: 15 μM **1** + DNA + Topo-I; Lane 6: 20 μM **1** + DNA + Topo-I; Lane 7: 25 μM **1** + DNA + Topo-I and (b) Docked model complex **1** (surface representation) towards the cleavage active site of Topo-I.

hypsochromic shift of 5 nm from the initial HSA emission intensity. The observed blue shift was mainly due to the fact that the active site in protein was buried in a hydrophobic environment [27]. These results indicated the interaction of complex **1** with HSA that lead to changes in its secondary structure (affecting the tryptophan residues of HSA).

In order to speculate the fluorescence quenching mechanism, the fluorescence quenching data at different temperatures (298, 309 and 319 K) were analyzed using the classical Stern–Volmer equation (Fig. S9a). The results revealed (Table S1) that the Stern–Volmer quenching constant K_{SV} was inversely correlated with temperature and k_q is larger than the limiting diffusion constant K_{dif} of the biomolecules ($K_{dif} = 2.0 \times 10^{10}$ M^{-1} s^{-1}) [28], indicating that fluorescence quenching was caused by a specific interaction between HSA and complex **1**, consistent with the static quenching mechanism (Scheme S1). Since, the static quenching mechanism was most probably preceded by complex formation; the quenching process was further analyzed according to the modified Stern–Volmer equation which revealed that binding constant decreased with increase in temperature. Furthermore, when small molecules bind independently to a set of equivalent sites on a macromolecule, the equilibrium between free and bound molecules was given by Eq. (4). And a plot of $\log[(F_o - F)/F]$ versus $\log[Q]$ was used to determine K (binding constant) and n (binding sites) as depicted in Fig. S9b which showed that K decreased with the increasing temperature but n increased along with rising of temperature, resulting in a reduction of the stability of complex **1**–HSA binding reaction (Table S2).

Thermodynamic parameters relying on temperatures were analyzed to determine the acting forces between drug molecules and biomacromolecules. There are essentially four types of non-covalent interactions such as electrostatic interactions, multiple hydrogen bonds, van der Waals interactions, hydrophobic contacts that played a key role in drug binding interaction [29]. The thermodynamic parameters, enthalpy change (ΔH), entropy change (ΔS) and free energy change (ΔG) are the main parameters to elucidate the binding mode of complex with HSA. From the thermodynamic standpoint, $\Delta H > 0$ and $\Delta S > 0$ imply a hydrophobic interaction; $\Delta H < 0$ and $\Delta S < 0$ reflect the van der Waals force or hydrogen bond formation; and $\Delta H \approx 0$ and $\Delta S > 0$ suggestive of an electrostatic forces [30]. The free energy change (ΔG) can be estimated from Eq. (6) based on the binding constants at different temperatures; 298, 309 and 319 K (Table S3). The ΔG and ΔH were negative, and ΔS was positive, indicating the formation of complex **1**–HSA was a spontaneous and exothermic process. Furthermore, the negative ΔH value (−8.68 kJ mol^{-1}) observed cannot be mainly attributed to electrostatic interactions since for electrostatic interactions ΔH is very small, almost zero (Fig. S10). Therefore, the negative ΔH and positive ΔS values suggest that hydrophobic and hydrogen bond interactions play major roles in the complex **1**–HSA binding reaction and contributed to the stability of the complex.

Fluorescence energy transfer occurs *via* overlapping of emission spectrum of a fluorophore (donor) with the absorption spectrum of another molecule (acceptor). The spectral overlap between the emission spectrum of donor (HSA) and the absorption spectrum of acceptor (complex **1**) was depicted in Fig. S11. According to Forster's theory, the rate of energy depends mainly on the following factors: (i) the extent of overlap between the donor emission and the acceptor absorption, (ii) the proper orientation of the transition dipole of donor and acceptor, and (iii) the distance between the donor and the acceptor molecules (Scheme S2). From Eqs. (7)–(9), the value of E, R_o, r and J were calculated and found to be 0.081, 3.97 nm, 5.94 nm and 1.14×10^{-13} M^{-1} cm^3, respectively. The donor to acceptor distance $r < 7$ nm indicated that the energy transfer from tryptophan residue in HSA to complex **1** occurred with high probability [31]. These results are consistent with the static quenching observed between complex **1** and HSA.

IR spectrum of proteins is typically used to determine conformational changes in the structure of proteins. Infrared spectra of proteins exhibited a number of amide bands that represented different vibrations of peptide moiety. The spectrum was obtained by subtracting the absorption of Tris buffer from the spectrum of HSA solution (Fig. S12). The protein amide bands have a relationship with the secondary structure of protein, and amide I band is more sensitive to the change of protein secondary structure than amide II and amide III. The evident peak shift of amide I band from 1613.1 to 1625.8 cm^{-1}, amide II band from 1558.3 to 1539 cm^{-1} and amide III band from 1242.3 to 1238.9 cm^{-1} revealed the interaction between complex **1** and HSA. These changes in these peak positions demonstrated that the secondary structure of HSA was changed upon the interaction resulting in the perturbation of amide vibrational frequencies [32]. These conformational changes of HSA in the presence of **1** were further monitored by 3D fluorescence spectral studies. As shown in Fig. 4, it was observed that the fluorescence intensities of peak **a** (Rayleigh scattering peak; $\lambda_{ex} = \lambda_{em}$) and peak **b** (280, 346 nm, λ_{ex}, λ_{em}; spectral behavior of the Trp residue) decreased significantly followed by quenching of fluorescence intensities induced by Trp residue of HSA.

The interaction of complex **1** with pBR322 DNA was monitored by using HPLC elution profiles in H_2O–Acetonitrile mixture at 270 nm. The chromatogram of complex **1** shows a broad peak and shoulder band observed at a retention time of 2.32 and 2.55 with relative intensity of 173,794 and 23,041, respectively (Fig. 5). The chromatograms of protein–DNA system (RT; 2.47 and 3.34) in the presence of complex **1** at different time intervals revealed the interaction of **1** with HSA and the release of the drug after a particular time interval approaching to DNA. It is, however, reasonable to assume that the presence of –GC– pair located in DNA favors specific binding of the Cu(II) ion to this particular site. These observations were consistent with our wet lab experiments viz., electrophoretic gel assay and spectroscopic investigations that the bonded drug with protein was released slowly in the presence of DNA and released drug moves towards the DNA duplex and free HSA was trying to achieve its original retention time towards native HSA (Fig. S13 and S14). On the basis of HPLC experiment it has been concluded that HSA work as carrier and DNA has its ultimate molecular target.

2.7. HSA photocleavage studies

In order to access the ability of the complex **1** to serve as a synthetic metalloproteases, the HSA photocleavage activity of the **1** was studied using 4 mM HSA in 50 mM Tris–HCl buffer on exposure to UV-A light of 365 nm (100 W) with different complex concentrations and varied exposure times (5–20 min) and the extent of protein photocleavage was compared with the untreated HSA band. As shown in Fig. 6, it was observed that HSA alone (Lane 1) did not show any apparent cleavage under these conditions. However, upon increasing the concentration of complex **1** (100–300 μM), HSA exhibited efficient cleavage activity with significant smearing or fading of the band on photoirradiation, indicating photocleavage of HSA under physiological reaction conditions. The fading out of the band suggests possible non-specific binding of the complex to HSA, leading to the cleavage into very small fragments as reported by Toshima and co-workers using porphyrin compounds [33]. Complex **1** did not show any protein cleavage activity in the dark, thus excluding the possibility of any hydrolytic protein damage.

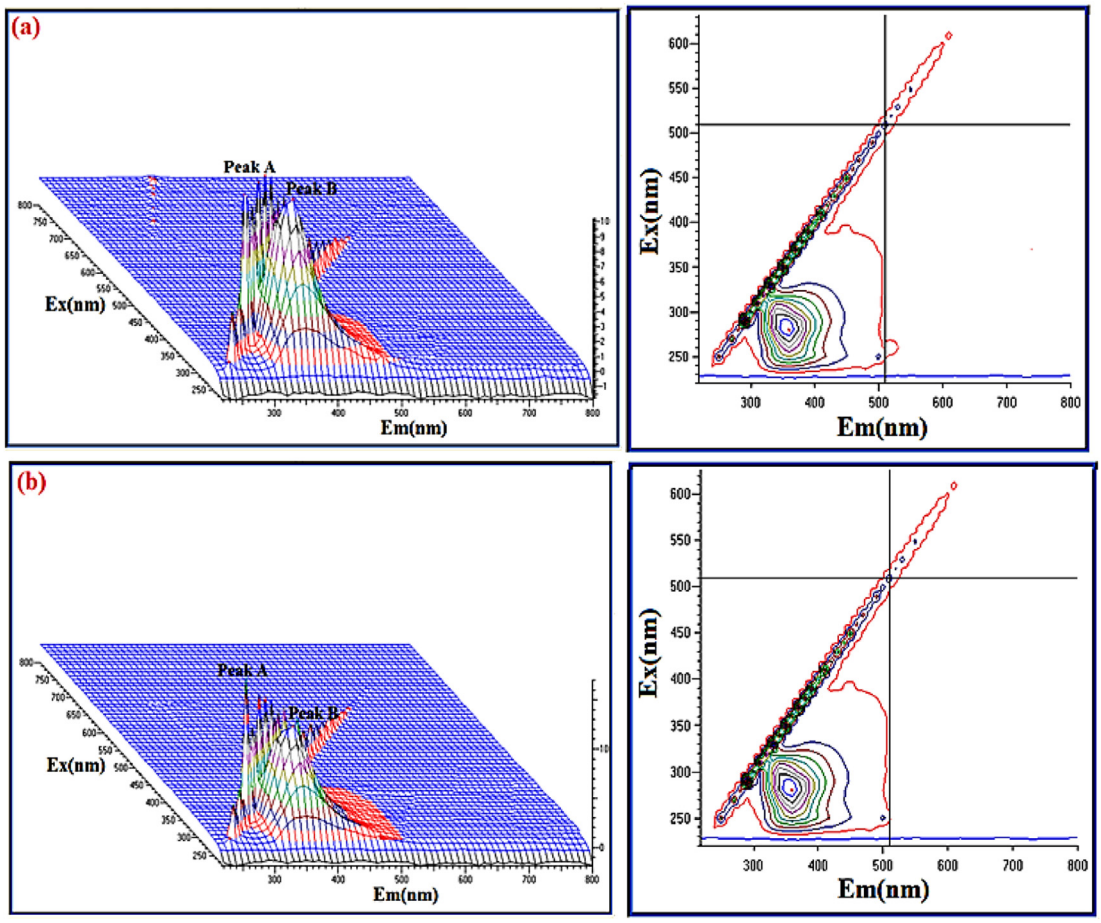

Fig. 4. 3D fluorescence spectrum and corresponding contour diagrams of (a) HSA, and (b) complex **1**-HSA system. The concentration of HSA is fixed at 1.5 mM and that of complex **1** is fixed at 12.5 mM. pH = 7.4, at room temperature.

To investigate the mechanism of photocleavage by reactive oxygen species (ROS) comparative HSA cleavage experiment of complex **1** was carried out in presence of standard radical scavengers such as DMSO and KI as hydroxyl radical scavenger (HO•), sodium azide (NaN_3) as singlet oxygen ($^1O_2$) quencher and SOD as superoxide radical scavenger were used prior to the exposure to UV-A light. The hydroxyl radical scavengers DMSO and KI did not show any obvious inhibition of photo-induced protein cleavage activity mediated by complex **1** thus indicating non-involvement of hydroxyl radicals as the reactive species. However significant

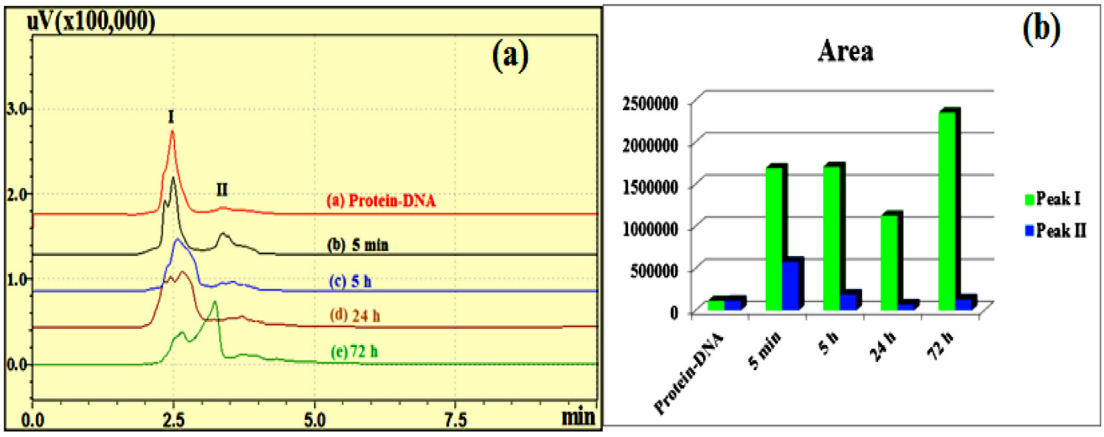

Fig. 5. (a) Time dependent HPLC chromatograms for the interaction of protein–DNA and complex **1** in 5 mM Tris HCl/50 mM NaCl buffer at pH 7.2. (b) Histogram showing the area of peaks for Protein–DNA interaction after the addition of **1** at different time intervals.

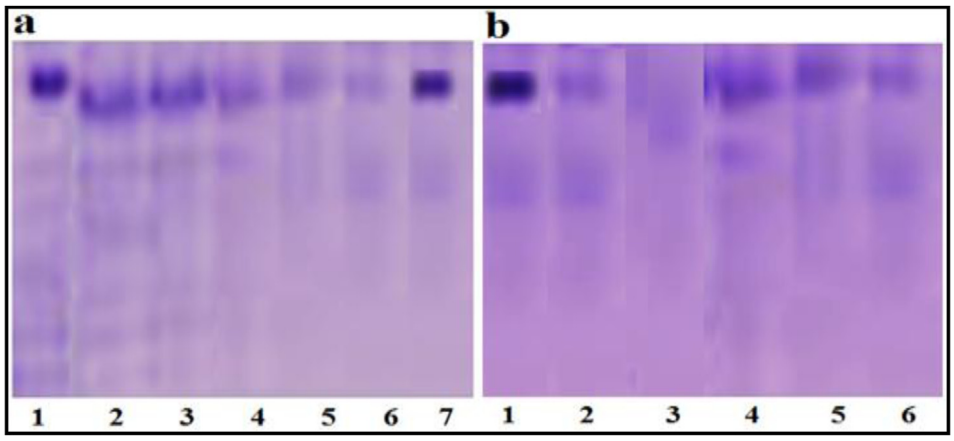

Fig. 6. SDS–PAGE electrophoresis in 12% polyacrylamide gel showing photocleavage of human serum album in (HSA, 15 μM) with 25 min photoexposure to UV-A1 light at 365 nm by complex **1** in Tris HCl buffer (pH 7.4), (a) at different concentration; lane 1, HSA control; Lane 2, HSA + **1** (100 μM); Lane 3, HSA + **1** (150 μM); Lane 4, HSA + **1** (200 μM); Lane 5, HSA + **1** (250 μM); Lane 6, HSA+ **1** (300 μM); Lane 7, HSA + **1** (300 μM, in the dark), (b) in the presence of standard radical scavengers; Lane 1, HSA + **1** (250 μM, in the dark); Lane 2, HSA + **1** (250 μM); Lane 3, HSA + DMSO (20 μL) + **1** (250 μM); Lane 4, HSA + NaN_3 (3 mM) + **1** (250 μM); Lane 5, HSA + SOD (15 units) + **1** (250 μM); Lane 6, HSA + KI (3 mM) + **1** (250 μM).

reduction in the photo-induced HSA cleavage activity was observed in presence of NaN_3 and SOD suggesting the photo-induced oxidative cleavage pathway [34].

2.8. Molecular docking studies with DNA and HSA

To ascertained the groove binding mode of complex **1** towards DNA, complex **1** was docked on DNA duplex of sequence d(CGCGAATTCGCG)$_2$ dodecamer (PDB ID: 1BNA). The resulting docked model showed that complex **1** localizes in the DNA minor groove within G–C rich region from chain B (G22 and C23B) through indole-3-propionic acid ligand and stabilized by van der Waal's interactions and hydrophobic contacts with DNA functional groups that define the groove (Fig. S15). The resulting relative binding energy of docked metal complex **1** DNA was found to be −306 eV. The more negative relative binding energy indicated that complex **1** strongly binds to the DNA, correlated well with the experimental DNA binding results.

Similarly, complex **1** was docked on molecular target HSA (pdb id: 1h9z) to understand the binding site at molecular level. Descriptions of the 3D structure of crystalline albumin have revealed that HSA comprises three homologous domains (denoted I, II, and III): I (residues 1–195) II (196–383) and III (384–585); each domain has two subdomains (A and B) that assemble to form heart shaped molecule. The principal region of drug binding sites of HSA are located in hydrophobic cavities in subdomain IIA and IIIA, corresponding to site I and site II, respectively and tryptophan residue (Trp-214) of HSA in subdomain IIA. The resulting docked model revealed that the complex **1** was inserted in the hydrophobic cavity of site I, and it was important to note that the tryptophan residue of HSA (Trp-214) was in close proximity with indole ring of complex **1**, suggesting the existence of hydrophobic interaction between them. Such finding provides a good structural basis to explain the very efficient fluorescence quenching of HSA emission in the presence of complex **1**. At the same time, there were considerable number of hydrogen bonds and electrostatic interactions due to the presence of several ionic and polar groups like Lys-195, Lys-199, Arg-218, His-242 and Glu-292 near the complex **1** (Fig. 7). On the other hand, the amino acid residues with aromatic ring could match with that of the phenanthroline ring of complex **1** in space in order to firm the binding environment of the complex **1**. Thus, we can conclude that there is a mutual complement between spectroscopic techniques and molecular modeling, which can

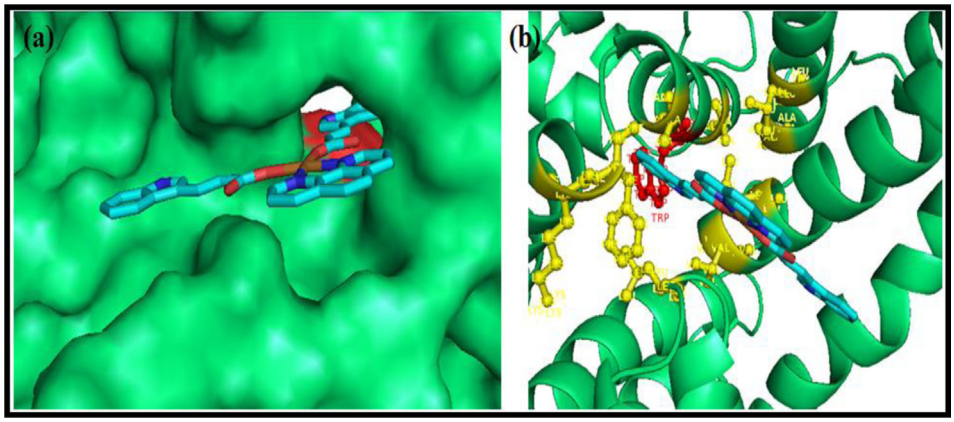

Fig. 7. Molecular docked model of (a) complex **1** (stick representation) located within the hydrophobic pocket in subdomain IIA of HSA. (b) The interaction mode between complex **1** (showing stick representation) and HSA (cartoon form).

Table 1
Summary of the screening data of complex **1** for the *in vitro* antitumor activity (in μg/ml).

Human tissue of origin		CNS	Ovarian	Leukemia	Colon	Breast	Prostate	Lung
Cell line		U373MG	A2780	K562	HCT15	MCF7	PC3	Hop62
GI_{50}	1	<10	<10	<10	<10	<10	<10	<10
	ADR	<10	<10	<10	<10	<10	<10	<10
TGI	1	<10	<10	16.6	75.6	20.8	25.3	<10
	ADR	16.9	<10	<10	78.4	27.3	60.0	26.4
LC_{50}	1	22.5	19.9	56.0	>80	56.9	62.8	36.1
	ADR	34.2	18.9	48.2	>80	64.3	>80	62.3

GI_{50} = Growth inhibition of 50% (GI_{50}) calculated from [(Ti − Tz)/(C − Tz)] × 100 = 50, drug concentration result in a 50% reduction in the net protein increase.
ADR = Adriamycin (taken as positive control compound).
GI_{50} value <10 μg/ml is considered to demonstrate activity.
TGI = Tumor growth inhibition.
LC_{50} = Lethal concentration of 50% (LC_{50}).

provide valuable information about the mode of interaction of the complex with DNA and the conformation constraints for adduct formation.

2.9. Antitumor activity assays

The *in vitro* activity of complex **1** was evaluated in terms of GI_{50}, TGI and LC_{50} (Table 1) values against seven different human carcinoma cell lines of different histological origin: U373MG (CNS), A2780 (Ovarian), K562 (Leukemia), HCT15 (Colon), MCF7 (Breast), PC3 (Prostate), Hop62 (Lung). The *in vitro* anti-tumor screening (Fig. 8) of **1** was evaluated as a consequence of their binding affinity towards DNA by applying microculture Sulforhodamine B test (SRB) [35]. The result showed high potential of the complex **1** as drug candidate, as expected from the *in vitro* DNA binding studies and topoisomerase I catalytic inhibition. The complex **1** exhibited very promising antitumor activity (GI_{50} < 10 μg/mL) against all these human carcinoma cell lines, indicating that it has the potential to act as efficacious metal-based anticancer drug.

2.10. Cell imaging studies

The cellular uptake of metal-based anticancer drugs is of importance for its effectiveness against tumors. In order to assess the intracellular localization of complex **1** inside the human cervical carcinoma (HeLa) cells, confocal microscopic experiments was performed as an initial investigation of its applicability as a fluorescent probe for live-cell applications. The fluorescence of the two species can be differentiated due to the different emission profiles. The emission from complex **1** alone was observed at 336 nm, while the DNA stain was observed at 450 nm. The incubation of HeLa cells with the complex **1** at 37 °C under a 5% CO_2 atmosphere resulted in efficient cellular uptake. To confirm its nuclear localization, the cell was subjected to staining for which the cell treated with complex **1** was thoroughly washed, stained with a blue nuclear dye, PI (Propidium Iodide), a DNA selective fluorescent probe and after fixation, the images were recorded (Figs. 9 and 10). The relative overlapping fluorescence intensities of compound and PI confirm the localization of compound with DNA. Further, the co-localization of compound **1** with PI, corroborates the interaction of this compound with DNA under live conditions. Hence, the live imaging studies revealed that Cu(II) complex act as a future potential chemotherapeutic agent.

3. Conclusion

In this work, we have synthesized and characterized a new Cu(II) molecular entity (**1**) derived from the 1,10-phenanthroline and Indole-3-propionic acid which was capable of minor groove

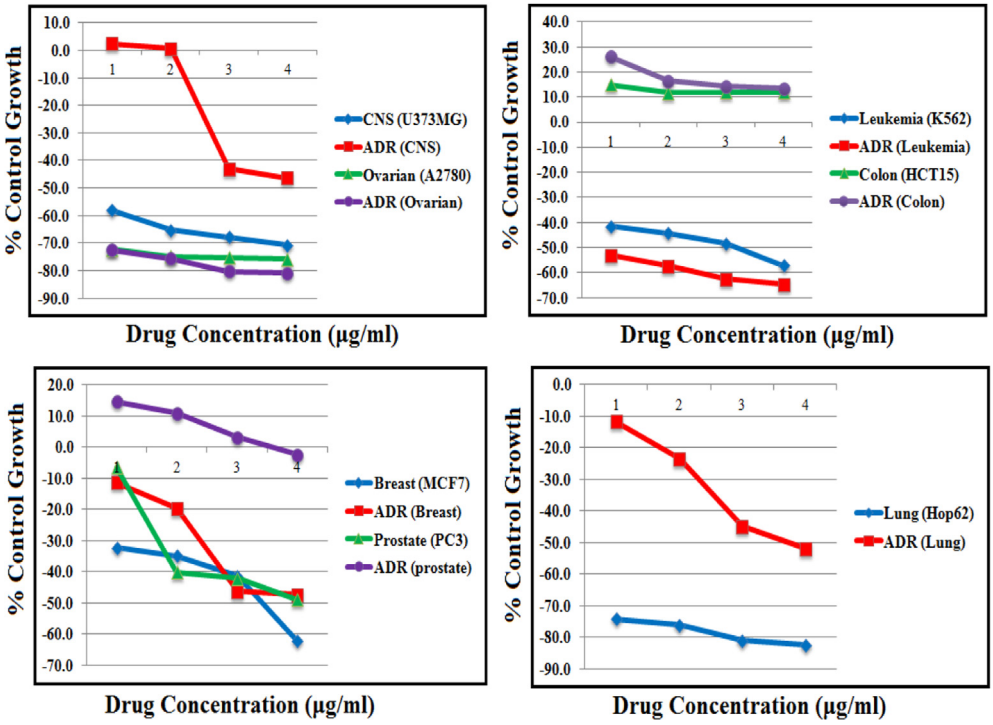

Fig. 8. Growth curve showing % Control growth verses Drug concentration (μg/ml) against different human carcinoma cell lines: U373MG (CNS), A2780 (Ovarian), K562 (Leukemia), HCT15 (Colon), MCF7 (Breast), PC3 (Prostate), Hop62 (Lung).

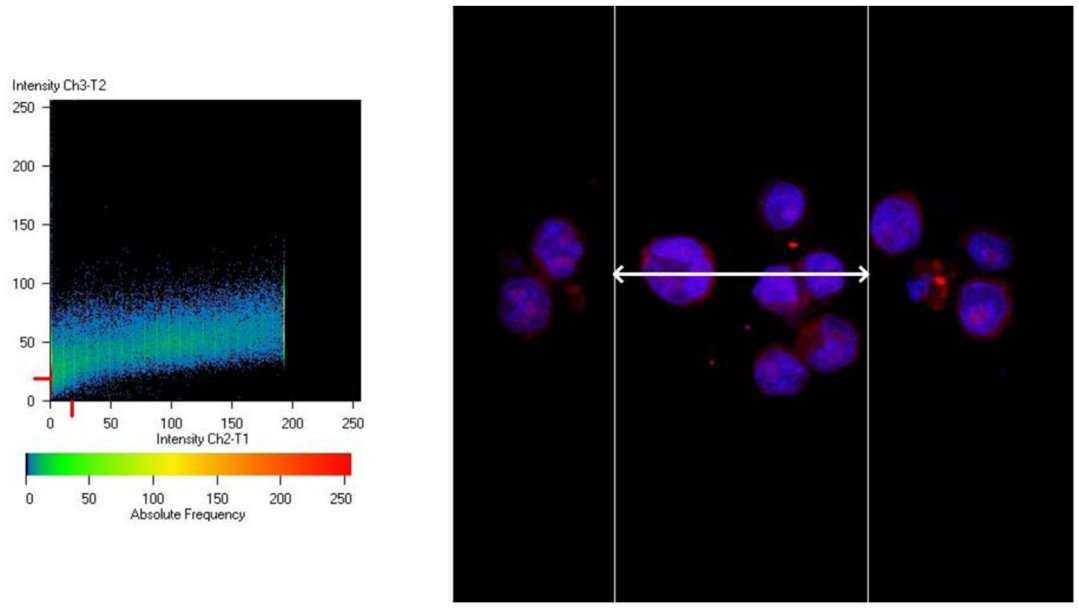

Number Pixels	Area [µm x µm]	Relative Area [%]	Mean Intensity Ch2-T1	Mean Intensity Ch3-T2	Standard Deviation Ch2-T1	Standard Deviation Ch3-T2	Overlap Coefficient	Correlation R	Correlation R x R
429009	7302.48	100.0	11	9	37	17	0.9	0.86	0.73

Fig. 9. Confocal study depicting colocalization of **1** with PI in live HeLa cells, suggesting **1** interacting with DNA similar to PI. Table shows good correlation of 1 with PI.

recognition of DNA and inhibited the catalytic activity of Topo-I. The complex **1** cleaves supercoiled plasmid DNA through an oxidative (O_2—pathway) cleavage mechanism induced by reactive oxygen species (ROS). Complex **1** showed potent *in vitro* cytotoxicity on U373MG, A2780, K562, HCT15, MCF7, PC3, Hop62 cancer cell lines; also confocal cell imaging studies using the HeLa cell line depicted its nuclear specific localization in the cells. Furthermore, affinity of complex **1** for HSA was investigated by

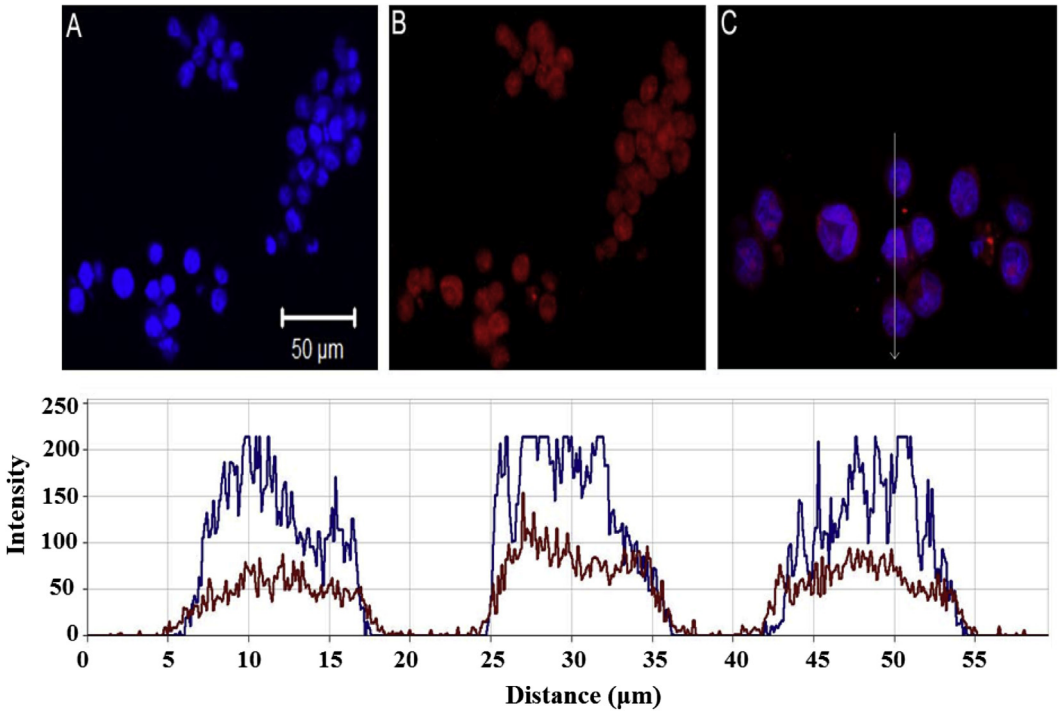

Fig. 10. Confocal projections showing localization of complex **1** (blue fluorescence in (B) and (C)) in HeLa cells, nucleus is counter stained with DNA specific dye propidium iodide (red fluorescence in (B) and (D)). Insets in (A), (B) and (C) clearly show the nucleus specific localization of **1** (A, C) and propidium iodide (B, C). Scale bar represents 50 µm. (For interpretation of the references to colour in this figure legend, the reader is referred to the web version of this article.)

means of employing UV–vis and fluorescence spectroscopy to understand the carrier role of serum albumin for such compound in blood under physiological conditions. Interestingly, the time dependent HPLC experiment revealed that bonded drug with protein releases slowly in the presence of DNA indicating that DNA was its ultimate molecular target.

4. Experimental section

4.1. Reagents and materials

All reagents were commercially available and used as supplied without further purification. Copper acetate monohydrate (Merck), Indole-3-propionic acid (Sigma–Aldrich), 1,10-Phenanthroline (Sigma–Aldrich) and Calf thymus DNA (CT DNA). Human DNA topoisomerase I, (Calbiochem), 6X loading dye (Fermental Life Science) and Supercoiled plasmid DNA pBR322 (Genei) were utilized as received.

HSA (fatty acid free, 99%) was purchased from Sigma and used without further purification. Acrylamide, N,N′-methylenebis–acrylamide, ammonium per sulfate, N,N,N′,N′-tetramethyl ethylenediamine (TEMED), 2-mercaptoethanol (MPE), glycerol, sodium dodecyl sulfate (SDS), bromophenol blue, coomassie brilliant blue R-250, tris(hydroxymethyl) aminomethane or Tris buffer from Sigma were used as received. The protein concentration was determined spectrophotometrically using an extinction coefficient of 35,219 M^{-1} cm^{-1} at 280 nm.

4.2. Methods and instrumentation

Carbon, hydrogen and nitrogen contents were determined on CHNSO Elemental Analyzer Elementar Vario EL III model. Molar conductance was measured at room temperature on CON 510 Bench conductivity TDS Meter. IR spectrum was recorded on Interspec 2020 FTIR spectrometer in KBr pellets from 400 to 4000 cm^{-1}. Electrospray mass spectra were recorded on Micromass Quattro II mass spectrometer. The EPR spectrum of the copper complex was acquired on a Varian E 112 ESR spectrometer using X-band frequency (9.5 GHz) at liquid nitrogen temperature in liquid state. Electronic spectrum was recorded on UV-1700 PharmaSpec UV–vis spectrophotometer (Shimadzu) in DMSO cuvettes of 1 cm path length. Fluorescence measurements were determined on a RF-5301 PC spectrofluorophotometer (Schimadzu). HPLC measurements were determined on a UFLC SPD 20A (Schimadzu). DNA and HSA cleavage experiments were performed with the help of Axygen made electrophoresis assembly, visualized and photographed by a Vilber–INFINITY gel documentation system.

4.3. Synthesis of [Cu(IPA)$_2$(Phen)]

To a stirred methanolic solution of Indole-3-propionic acid (2 mmol, 0.378 g) was added $Cu(CH_3COO)_2.H_2O$ (1 mmol, 0.199 g) dissolved in methanol dropwise. The resulting solution was refluxed for 6 h and subsequently a methanolic solution of 1,10-phenanthroline (1 mmol, 0.198 g) dissolved in methanol was added to it. The resulting solution was further refluxed for 3 h and was reduced to 5 ml by rotatory evaporator. Dark green colored crystals of complex were collected from the above concentrated solution at room temperature (Scheme 1).

Yield: 80%, M.P 180 °C. Analysis calculated for $[C_{34}H_{28}CuN_4O_4]$ (%): C, 65.85; H, 4.55; N, 9.03 Found: C, 65.83; H, 4.42; N, 9.04. IR (KBr, υ_{max}/cm^{-1}): 1337 υ_s(COO); 1587 υ_{as}(COO); 849, 714 ν(C–H) phen; 563 υ(Cu–O); 424 υ(Cu–N). Molar conductance: Λ_M (1×10^{-3} M, DMSO): 11 Ω^{-1} cm^2 mol^{-1} (non-electrolyte). UV–vis. (1×10^{-3} M, DMSO, nm): 270, 367, 540. ESI–MS (m/z, DMSO): 620.43$[C_{34}H_{28}CuN_4O_4]^+$.

4.4. Single-crystal X-ray studies

Single crystal X-ray data of complex **1** was collected at 100 K on a Bruker SMART APEX CCD diffractometer using graphite monochromated MoK$_\alpha$ radiation ($\lambda = 0.71073$ Å). The linear absorption coefficients, scattering factors for the atoms and the anomalous dispersion corrections were referred from the International Tables for X-ray Crystallography [36]. The data integration and reduction were worked out with SAINT [37] software. Empirical absorption correction was applied to the collected reflections with SADABS [38], and the space group was determined using XPREP [39]. The structure was solved by the direct methods using SHELXTL-97 [40] and refined on F^2 by full-matrix least-squares using the SHELXTL-97 programme [41] package. Only a few H atoms could be located in the difference Fourier maps in the structure. The rest were placed at calculated positions using idealized geometries (riding model) and assigned fixed isotropic displacement parameters. All non-H atoms were refined anisotropically. The crystal and refinement data are collected in Table 2. Selective bond distances and angles are given in Table S4.

4.5. DNA binding and cleavage experiments

DNA binding experiments include absorption spectral traces and emission spectroscopy conformed to the standard methods and practices previously adopted by our laboratory whereas DNA cleavage experiment has been performed by the standard protocol [42–45]. While measuring the absorption spectra an equal amount of DNA was added to both the compound solution and the reference solution to eliminate the absorbance of the CT DNA itself, and Tris buffer was subtracted through base line correction.

Table 2
Crystal and structure refinement data for **1**.

Parameters	**1**
Formula	$C_{34}H_{28}CuN_4O_4$
Fw (g mol^{-1})	620.14
Crystal system	Monoclinic
Space group	*P21/n*
a (Å)	21.868 (5)
b (Å)	12.879 (3)
c (Å)	22.309 (5)
α (deg)	90.00
β (deg)	113.871 (5)
γ (deg)	90.00
U (Å^3)	5746 (3)
Z	8
ρ_{calc} (g/cm^3)	1.434
μ (mm^{-1})	0.807
F (000)	2568
Crystal size (mm)	0.23 × 0.19 × 0.16
Temp (K)	100 (2)
Measured reflns	37,229
Unique reflns	5641
θ Range (deg)/completeness (%)	2.00 to 25.16/0.994
GOF[a]	0.999
Final R[b] indices	$R1 = 0.0769$
$[I > 2\sigma(I)]$	w$R2 = 0.1616$
R^b indices	$R1 = 0.1577$
(all data)	w$R2 = 0.1990$
largest diff. peak/hole (e.Å^{-3})	1.337/−1.517
CCDC	942,513

[a] GoF is defined as $\{\sum[w(F_0^2 - F_c^2)]/(n-p)\}^{1/2}$ where n is the number of data and p is the number of parameters.
[b] $R = \{\sum||F_0| - |F_c||/\sum|F_0|\}$, $wR_2 = \{\sum w(F_0^2 - F_c^2)^2/\sum w(F_0^2)^2\}^{1/2}$.

4.6. HSA binding studies

Absorption spectra were recorded on a Shimadzu UV-1700 pharmaspec UV–Vis spectrophotometer using cuvettes of 1 cm path length. HSA concentration was determined from absorption spectra, taking the absorbance of a 1 mg ml^{-1} solution at 280 nm (λ_{max} Trp-214) as 1.80×10^{-6} M. The value of binding constants can be calculated from the method which was described earlier [46].

4.6.1. Fluorescence quenching studies with HSA

Fluorescence measurements were carried out on Hitachi F–2500 fluorescence spectrophotometer in a 1 cm path-length quartz cell with the excitation and emission wavelength set at 280 and 300–400 nm, respectively. The interaction of complex ($0.67–1.67 \times 10^{-5}$ M) with HSA content of fixed concentration (0.67×10^{-6} M) was studied. The intensity at 362 nm (Tryptophan) was used to calculate the binding constant (K). The fluorescence quenching of HSA at different temperatures (299, 308 and 318 K) were determined using the Stern–Volmer equation (Eq. (1)) [47]:

$$\frac{F_o}{F} = 1 + K_q \tau_o [Q] = 1 + K_{sv}[Q] \quad (1)$$

Where F_o and F are the fluorescence intensities in absence and presence of quencher, respectively, [Q] is the quencher concentration, and K_{SV} Stern–Volmer quenching constant, which can be written as:

$$K_q = \frac{K_{SV}}{\tau_o} \quad (2)$$

Where k_q is the biomolecular quenching rate constant and so is the average lifetime of the fluorophore (Trp–214) in absence of quencher and its value is around 10^{-8} s for most biomolecules [48]. Therefore, Eq. (1) was applied to determine K_{sv} by linear regression of a plot of F_o/F versus [Q].

4.6.2. Calculation of binding constant

The binding constant was calculated from the modified Stern–Volmer equation (Eq. (3))

$$\frac{1}{[F_o - F]} = \frac{1}{F_o} + \frac{1}{K_b}\frac{1}{F_o}\frac{1}{Q} \quad (3)$$

Where K_b is the binding constant of complex **1** with biomolecules which was calculated from the intercept and slope of slopes of the Lineweaver–Burk ($1/(F_o - F)$ versus $1/[Q]$) (intercept = $1/F_o$, slope = $1/K_b F_o$, so K_b = intercept/slope). Furthermore, the binding constant (K) and number of bound complex **1** to HSA (n) were determined by plotting the double log graph of the fluorescence data using (Eq. (4)).

$$\log\left[\frac{F_o - F}{F}\right] = \log K + n \log[Q] \quad (4)$$

4.6.3. Determination of thermodynamic parameters

The thermodynamic parameters can be calculated from the Van't Hoff equation (Eq. (5))

$$\ln K = \frac{-\Delta H}{RT} + \frac{\Delta S}{R} \quad (5)$$

where K is the Lineweaver–Burk static quenching constant at the corresponding temperature and R is the gas constant, in which ΔH and ΔS of reaction could be determined from the linear relationship between ln K and the reciprocal absolute temperature (Fig. S5, ESI w). Furthermore, the free energy change (ΔG) was calculated by the following equation:

$$\Delta G = \Delta H - T\Delta S = -RT \ln K \quad (6)$$

4.6.4. Calculations of energy transfer

A Forster resonance energy transfer (FRET) mechanism (Fig. 3) is involved in the quenching of Trp fluorescence by complex **1**, the efficiency of energy transfer (E) is given by Ref. [49]:

$$E = 1 - \frac{F}{F_o} = \frac{R_o^6}{R_o^6 + r_o^6} \quad (7)$$

where F and F_o are the fluorescence intensities of HSA in the presence and absence of quencher, r is the distance between acceptor and donor and R_o is the critical distance when the transfer efficiency is 50%. The value of R_o can be calculated using the following equation:

$$R_o^6 = 8.78 \times 10^{-25} K^2 N^{-4} \varphi J \quad (8)$$

where K^2 is the spatial orientation factor between the emission dipole of the donor and the absorption dipole of the acceptor, N is the refractive index of the medium, ϕ is the fluorescence quantum yield of the donor and J is the overlap integral of the fluorescence emission spectrum of the donor and the absorption spectrum of the acceptor and is calculated by the following Eq. (9):

$$J = \frac{\int_0^\infty F(\lambda)\varepsilon(\lambda)\lambda^4 \Delta\lambda}{\int_0^\infty F(\lambda)\Delta\lambda} \quad (9)$$

where $F(\lambda)$ is the corrected fluorescence intensity of the donor at wavelength λ and $\varepsilon(\lambda)$ is the molar absorption coefficient of the acceptor at wavelength λ. Under the experimental condition, $K^2 = 2/3$, $N = 1.336$, $\phi = 0.188$ [50].

Fourier transform infrared measurements were carried out on an Interspec 2020 FTIR spectrometer and were recorded in liquid phase in the 450–4000 cm^{-1} range.

4.7. HSA photocleavage studies

Photo-induced protein cleavage experiments were performed by following the standard methods and practices previously adopted by Kumar and co-workers [51]. The photo-induced protein cleavage studies were carried out using freshly prepared solution of HSA in 50 mM Tris–HCl buffer (pH 7.4). The protein solutions (15 μM) containing complex **1** with increasing concentrations of 100–300 μM were photo-irradiated at 365 nm for 25 min incubation at 37 °C followed by SDS–PAGE analysis.

4.8. Molecular docking

The rigid molecular docking studies were performed by using HEX 6.3 software [52], which is an interactive molecular graphics program for calculating and displaying feasible docking modes of protein. The Hex 6.3 performs protein docking using Spherical Polar Fourier Correlations (Ritche and Venkataraman, 2010). Hex 6.3 necessitates the ligand and the receptor as input in PDB format. The parameters used for docking include: correlation type – shape only, FFT mode – 3D, grid dimension – 0.6, receptor range – 180, ligand range – 180, twist range – 360, distance range – 40. The

coordinates of complex **1** were taken from its crystal structure as a cif file and were converted to the PDB format using Mercury software. The crystal structure of the B-DNA dodecamer d(CGCGAATTCGCG)$_2$ (PDB ID: 1BNA), human–DNA–Topo-I (PDB ID: 1SC7) and human serum albumin (PDB ID: 1h9z) was downloaded from the protein data bank (http://www.rcsb.org./pdb). All calculations were carried out on an Intel Pentium 4, 2.4 GHz based machine running MS Windows XP SP2 as the operating system. Visualization of the docked pose has been done by using PyMol (http://pymol.sourceforge.net/) molecular graphic program.

4.9. Topoisomerase I inhibition assay

One unit of the enzyme was defined as completely relaxed 1 μg of negatively supercoiled pBR322 DNA in 30 min at 310 K under the standard assay conditions. The reaction mixture (30 μL) contained 35 mM Tris–HCl (pH 8.0), 72 mM KCl, 5 mM $MgCl_2$, 5 mM DTT, 2 mM spermidine, 0.1 mg mL^{-1} BSA, 0.25 μg pBR322 DNA, 2 Unit Topo-I and complex **1**. These reaction mixtures were incubated at 310 K for 30 min, and the reaction was terminated by addition of 4 μL of 5× buffer solution consisting of 0.25% bromophenol blue, 4.5% SDS and 45% glycerol. The samples were electrophoresed through 1% agarose in TAE at 30 V for 8 h.

5. Antitumor activity assays

The following cell lines were used for *in vitro* antitumor screening; U373MG (CNS), A2780 (Ovarian), K562 (Leukemia), HCT15 (Colon), MCF7 (Breast), PC3 (Prostate), Hop62 (Lung). Human malignant cell lines were procured and grown in RPMI–1640 medium supplemented with 10% Fetal Bovine Serum (FBS) and antibiotics to study growth pattern of these cells. The proliferation of the cells upon treatment with chemotherapy was determined by means of the Sulphorhodamine-B (SR-B) semi-automated assay. All cell lines were seeded into 96 well plates and cells were counted and cell count was adjusted according to the titration readings so as to give optical density in the linear range (from 0.5 to 1.8) and were incubated at 37 °C in CO_2 incubator for 24 h. The stock solution of the complex were prepared as 100 mg/mL in DMSO and four dilutions i.e. 10 μL, 20 μL, 40 μL, 80 μL, in triplicates were tested, each well receiving 90 μL of cell suspension. The plates were labeled properly and were incubated for 48 h. Termination of experiment was done by gently layering the cells with 50 μL of chilled 30% TCA (in case of adherent cells) and 50% TCA (in case of suspension cell lines) for cell fixation and kept at 4 °C for 1 h. Plates stained with 50 μL of 0.4% SRB for 20 min. All experiments were made in triplicate.

5.1. Nuclear localization by live cell imaging study

HeLa cells were grown in a culture flask containing DMEM (Delbeco Modified Eagle's Medium) supplemented with 10% FBS (Fetal Bovine Serum) and 5% CO_2 at 37 °C. Cells were trypsinized with 0.05% trypsin–EDTA (GIBCO–25,300) for 2 min followed by addition of 1 mL of fresh DMEM medium containing serum to inhibit trypsin activity. Cells were spun at 1200 rpm for 10 min and the sediment was suspended in 1xPBS (pH 7.4), placed on poly-lysine coated slides and incubated for one hour at room temperature for adherence. Cells were incubated with complex **1** (40 μM) for 60 min in dark, washed twice with 1xPBS for 5 min each and then incubated with Propidium Iodide (1 μg/mL, Sigma, P4864) for 5 min followed by washing twice with 1 × PBS. Cells were mounted in DABCO (Sigma, USA) and observed under EC Plan–Neofluar 40×/1.30 DIC M27 oil objective lens using ZEISS LSM–510 Meta confocal microscope. Fluorescence emissions were recorded for compound and PI using Blue Diode 405 and HeNe 561 laser line, respectively.

Acknowledgments

We gratefully acknowledge the financial support received from the DST–PURSE programme and DRS–1 (SAP) from UGC, New Delhi, India and author Mehvash Zaki is highly thankful for SRF from CSIR India for the financial support.

Appendix A. Supplementary data

Supplementary data related to this article can be found at http://dx.doi.org/10.1016/j.ejmech.2014.06.018.

References

[1] T. Helleday, E. Petermann, C. Lundin, B. Hodgson, R.A. Sharma, Nat. Rev. Cancer 8 (2008) 193–204.
[2] B. Rosenberg, L. Vancamp, T. Krigas, Nature 205 (1965) 698–699.
[3] B. Rosenberg, E. Renshaw, L. Vancamp, J. Hartwick, J. Drobnik, J. Bacteriol. 93 (1967) 716–721.
[4] L. Kelland, Nat. Rev. Cancer 7 (2007) 573–584.
[5] T. Afrati, A.A. Pantazaki, C.D. Samara, C. Raptopoulou, A. Terzis, D.P. Kessissoglou, Dalt. Trans. 39 (2010) 765–775.
[6] M.J. Burkitt, Methods Enzymol. 234 (1994) 66–79.
[7] (a) L. Li, K. Du, Y. Wang, H. Jia, X. Hou, H. Chao, L. Ji, Dalt. Trans. 42 (2013) 11576–11588;
(b) M.G. Alvarez, A.P. Alvarez, L.D.C. Agudo, A. Castineiras, M.L. Gonzalez, J. Borrasa, G.A. Pina, Dalt. Trans. 42 (2013) 10244–10259.
[8] P.U. Maheswari, S. Roy, H.d. Dulk, S. Barends, G.v. Wezel, B. Kozlevcar, P. Gamez, J. Reedijk, J. Am. Chem. Soc. 128 (2006) 710–711.
[9] A.R. Saundane, V.T. Katkar, A.V. Vaijinath, Hindawi Publ. Corp. J. Chem. 2013 (2013) 530135–530144.
[10] (a) M. Karbownik, J.J. Garcia, A. Lewinski, R.J. Reiter, J. Bioenerg. Biomemb. 33 (2001) 73–78;
(b) P. Lukose, S.C. Bhatia, A.K. Narula, J. Organomet. Chem. 403 (1991) 153–157.
[11] (a) C. Bailly, Curr. Med. Chem. 7 (2000) 39–58;
(b) M.K. Kathiravan, M.M. Khilare, A.S. Chothe, M.A. Nagras, J. Chem. Biol. 6 (2013) 25–36.
[12] X. Xiao, X. Han, Z. Mei, D. Zhua, K. Shao, J. Liang, M. Tiana, L. Xu, J. Organomet. Chem. 729 (2013) 28–39.
[13] S. Tabassum, M. Afzal, F. Arjmand, J. Photochem. Photobiol. B 115 (2012) 63–72.
[14] S.P. Perlepes, J.C. Huffman, G. Christou, Polyhedron 14 (1995) 1073–1081.
[15] R. Buchtik, Z. Travnicek, J. Vanco, R. Herchel, Z. Dvorak, Dalt. Trans. 40 (2011) 9404–9412.
[16] T. Fujii, A. Naito, S. Yamaguchi, A. Wada, Y. Funahashi, K. Jitsukawa, S. Nagatomo, T. Kitagawa, H. Masuda, Chem. Commun. (2003) 2700–2701.
[17] R.S. Kumar, K. Sasikala, S. Arunachalam, J. Inorg. Biochem. 102 (2008) 234–241.
[18] S. Sujatha, S. Balasubramanian, B. Varghese, M. Jayaprakashvel, N. Mathivanan, Inorg. Chim. Acta 386 (2012) 109–115.
[19] M. Chauhan, K. Banerjee, F. Arjmand, Inorg. Chem. 46 (2007) 3072–3082.
[20] N. Shahabadi, S. Kashanian, F. Darabi, Eur. J. Med. Chem. 45 (2010) 4239–4245.
[21] W.B. Devi, R.K.B. Singh, J.P. Jasinski, J.A. Golen, Inorg. Chem. Commun. 21 (2012) 163–167.
[22] D.S. Raja, E. Ramachandran, N.S.P. Bhuvanesh, K. Natarajan, Eur. J. Med. Chem. 64 (2013) 148–159.
[23] H. Wu, J. Yuan, Y. Bai, G. Pan, H. Wang, J. Kong, X. Fan, H. Liu, Dalt. Trans. 41 (2012) 8829–8838.
[24] R. Rao, A.K. Patra, P.R. Chetana, Polyhedron 27 (2008) 1343–1352.
[25] S. Tabassum, A. Asim, F. Arjmand, M. Afzal, V. Bagchi, Eur. J. Med. Chem. 58 (2012) 308–316.
[26] G.S. Laco, J.R. Collins, B.T. Luke, H. Kroth, J.M. Sayer, D.M. Jerina, Y. Pommier, Biochemistry 41 (2002) 1428–1435.
[27] E. Ramachandran, D.S. Raja, N.S.P. Bhuvanesh, K. Natarajan, Dalt. Trans. 41 (2012) 13308–13323.
[28] S. Sanyakamdhorn, D. Agudelo, H.-A. Tajmir-Riahi, Biomacromolecules 14 (2013) 557–563.
[29] Y.-Z. Zhang, X. Xiang, P. Mei, J. Dai, L.-L. Zhang, Y. Liu, Spectrochim. Acta A 72 (2009) 907–914.
[30] A. Manna, S. Chakravorti, Mol. Biosyst. 9 (2013) 246–257.
[31] C. Li, F. Cui, R. Mao, R. Huo, G. Qu, Org. Biomol. Chem. 10 (2012) 869–875.
[32] S. Tabassum, W.M. Al-Asbahy, M. Afzal, F. Arjmand, R.H. Khan, Mol. Biosyst. 8 (2012) 2424–2433.
[33] S. Tanimoto, D. Takahashi, K. Toshima, Chem. Commun. 48 (2012) 7659–7671.

[34] M. Roy, T. Bhowmick, R. Santhanagopal, S. Ramakumar, A.R. Chakravarty, Dalt. Trans. (2009) 4671–4682.
[35] T. Lammers, P. Peschke, V. Ehemann, J. Debus, B. Slobodin, S. Lavi, P. Huber, Mol. Cancer 6 (65) (2007) 1–14.
[36] International Tables for X-ray Crystallography vol. III, Kynoch Press, Birmingham, England, 1952.
[37] SAINT, Version 6.02, Bruker AXS, Madison, WI, 1999.
[38] G.M. Sheldrick, SADABS: Empirical Absorption Correction Program, University of Gottingen, Göttingen, Germany, 1997.
[39] XPREP, Version 5.1, Siemens Industrial Automation Inc., Madison, WI, 1995.
[40] G.M. Sheldrick, SHELXTL Reference Manual, Version 5.1, Bruker AXS, Madison, WI, 1997.
[41] G.M. Sheldrick, SHELXL–97: Program for Crystal Structure Refinement, University of Gottingen, Gottingen, Germany, 1997.
[42] F. Arjmand, S. Parveen, M. Afzal, L. Toupet, T.B. Hadda, Eur. J. Med. Chem. 49 (2012) 141–150.
[43] F. Arjmand, F. Sayeed, S. Parveen, S. Tabassum, A.S. Juvekar, S.M. Zingde, Dalt. Trans. 42 (2013) 3390–3401.
[44] F. Arjmand, M. Muddassir, Y. Zaidi, D. Ray, Med. Chem. Commun. 4 (2013) 394–405.
[45] F. Arjmand, F. Sayeed, M. Muddassir, J. Photochem. Photobiol. B 103 (2011) 166–179.
[46] J.J. Stephanos, J. Inorg. Biochem. 62 (1996) 155–169.
[47] L. Trynda-Lemiesz, B.K. Keppler, H. Koztowski, J. Inorg. Biochem. 73 (1999) 123–128.
[48] M.R. Eftink, Fluorescence Quenching Reaction: Probing Biological Macromolecular Structures, Biophysical and Biochemical Aspects of Fluorescence Spectroscopy, Plenum Press, New York, 1991.
[49] T. Förster, O. Sinanoglu (Eds.), Modern Quantum Chemistry, vol. 3, Academic Press, New York, 1996, pp. 93–138.
[50] A. Sharma, S.G. Schulman, Introduction to Fluorescence Spectroscopy, John Wiley & Sons, Inc., New York, 1999.
[51] (a) C.V. Kumar, A. Buranaprapuk, G.J. Opiteck, M.B. Moyer, S. Jockusch, N.J. Turro, Proc. Natl. Acad. Sci. U. S. A. 95 (1998) 10361–10366;
(b) A. Buranaprapuk, S.P. Leach, C.V. Kumar, J.R. Bocarsly, Biochim. Biophys. Acta 1387 (1998) 309–316.
[52] D.W. Ritche, V. Venkataraman, Bioinformatics 26 (2010) 2398–2405.